Monthly Notices
of the
ROYAL ASTRONOMICAL SOCIETY

Mon. Not. R. Astron. Soc. **422,** 1914–1921 (2012) doi:10.1111/j.1365-2966.2011.20356.x

Spectral analysis of 1H 0707−495 with *XMM–Newton*

T. Dauser,[1⋆] J. Svoboda,[2,3] N. Schartel,[3] J. Wilms,[1] M. Dovčiak,[2] M. Ehle,[3] V. Karas,[2] M. Santos-Lleó[3] and H. L. Marshall[4]

[1]*Dr Karl Remeis-Observatory and Erlangen Centre for Astroparticle Physics, Sternwartstr. 7, 96049 Bamberg, Germany*
[2]*Astronomical Institute, Academy of Sciences, Boční II 1401, CZ-141 31 Prague, Czech Republic*
[3]*XMM–Newton Science Operations Centre, ESA, Villafranca del Castillo, Apartado 78, 28691 Villanueva de la Cañada, Spain*
[4]*Kavli Institute for Astrophysics and Space Research, Massachusetts Institute of Technology, 77 Massachusetts Avenue, Cambridge, MA 02139, USA*

Accepted 2011 December 7. Received 2011 December 6; in original form 2011 October 4

ABSTRACT

We present the results of a 500 ks long *XMM–Newton* observation and a 120 ks long quasi-simultaneous *Chandra* observation of the Narrow-Line Seyfert 1 galaxy 1H 0707−495 performed in 2010 September. Consistent with earlier results by Fabian et al. and Zoghbi et al., the spectrum is found to be dominated by relativistically broadened reflection features from an ionized accretion disc around a maximally rotating black hole. Even though the spectra changed between this observation and earlier *XMM–Newton* observations, the physical parameters of the black hole and accretion disc (i.e. spin and inclination) are consistent between both observations. We show that this reflection spectrum is slightly modified by absorption in a mildly relativistic, highly ionized outflow which changed velocity from around 0.11 c to 0.18 c between 2008 January and 2010 September. Alternative models, in which the spectral shape is dominated by absorption, lead to spectral fits of similar quality, however, the parameters inferred for the putative absorber are unphysical.

Key words: galaxies: active – galaxies: individual: 1H 0707−495 – galaxies: nuclei – X-rays: galaxies.

1 INTRODUCTION

The Narrow-Line Seyfert 1 galaxy 1H 0707−495 ($z = 0.04057$; Jones et al. 2009) is most famous for its huge and sharp drop in flux at ∼7 keV. Discovered by Boller et al. (2002), this feature was initially interpreted as an absorption edge despite the lack of a fluorescent emission line. Subsequent models for the feature included partial covering by a thick absorber (Tanaka et al. 2004), which also explains the temporal changes seen in its location (Gallo et al. 2004). In a long *XMM–Newton* observation, however, Fabian et al. (2009) and Zoghbi et al. (2010) showed that relativistically broadened fluorescent iron Kα emission is a more likely explanation, especially given that these authors could also show that the source's soft excess can be modelled by a relativistic iron Lα line, the first one ever observed. That the position of the two lines and the ratio of the normalizations agree with expectations adds further evidence to the reflection scenario (Fabian et al. 2009). In order to produce such a strong feature and an observable Fe Lα line, the iron abundance in 1H 0707−495 has to be several times the solar composition. The new observations also ruled out the partial covering explanation for the feature, as the strong absorption lines and edges predicted by these models are not compatible with high-resolution X-ray spectra (Zoghbi et al. 2010). Recently, Fabian et al. (2012) observed 1H 0707−495 at low flux, confirming the reflection-dominated interpretation. The same physical interpretation also successfully describes the spectra of similar active galactic nuclei (AGN), e.g. IRAS 13224−3809 (Boller et al. 2003; Ponti et al. 2010), too.

In this paper we analyse data of 1H 0707−495 taken by the *XMM–Newton* satellite from 2010 September 12 until 2010 September 19. The results are compared to a previous observation (Fabian et al. 2009; Zoghbi et al. 2010) with similar exposure and flux. Section 2 is dedicated to present the data reduction we applied and general properties of the observation are discussed. The outcome of our spectral modelling is presented in Section 3, and finally the results are discussed in Section 4.

2 DATA ANALYSIS

We analyse data of 1H 0707−495 from a ∼500 ks long observing run of *XMM–Newton* satellite (Jansen et al. 2001) from 2010 September 12 until 2010 September 19 [*XMM–Newton* revolutions (Revs) 1971–1974, corresponding to the Obs IDs 0653510301, 0653510401, 06535105010 and 653510601]. These data are then compared to ∼500 ks of measurements from an earlier *XMM–Newton* observation of the source performed from 2008 January 29 to 2008 February 6. We concentrate on data from the European

⋆E-mail: thomas.dauser@sternwarte.uni-erlangen.de

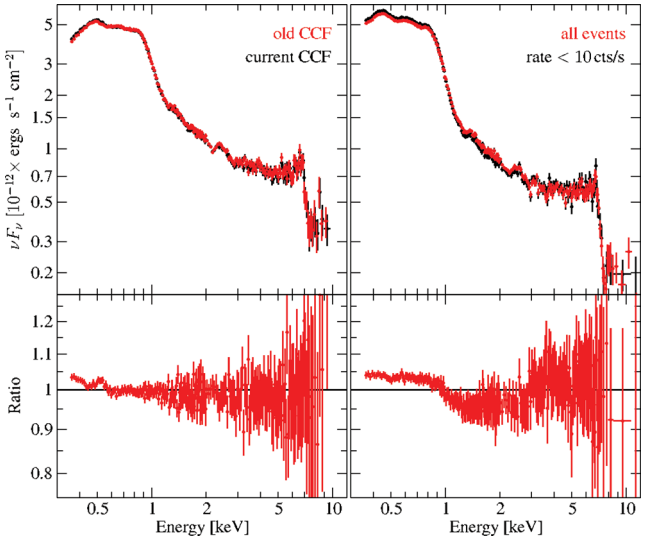

Figure 1. Left: comparison of the extractions for Revs 1491–1494 between the current calibration of the EPIC-pn (black, calibration date 2011 September 13) and the older version (red, 2009 July 1). The bottom figure shows the ratio between the data sets. Right: spectra of Revs 1971–1974 obtained for a 'normal' extraction (red) and an extraction with the conditions RATE < 10 (black). All spectra are normalized in flux to the 'black' spectra.

Photon Imaging Camera (EPIC)-pn (Strüder et al. 2001) and the reflection grating spectrometer (RGS; den Herder et al. 2001). Data were reduced using the *XMM–Newton* Software Analysis System (SAS, v.11.0.0) and the newest calibration files.

Both sets of observations were analysed in the same way. We merged the linearized event files of the four consecutive observations to a single event file. These data were cleaned for high background times following Schartel et al. (2007) and Piconcelli et al. (2005), resulting in final exposure times of 328 and 410 ks for Revs 1491–1494 and Revs 1971–1974, respectively. The EPIC-pn source spectra were extracted from a circular region with a radius of 36 arcsec centred on the maximum of source emission. In order to avoid any issues due to background Cu K emission lines from the electronic circuits on the back side of the detector (see Zoghbi et al. 2010), background data were taken from a different chip, using a circular region of the same size at a CCD position located at a similar distance from the readout node as the source position (see 'XMM–Newton Users Handbook', Issue 2.9, 2011, ESA, XMM–Newton SOC).

In order to exclude any contamination of the spectra due to pile up, a light curve with a resolution of 40 s was generated and only times with count rates below 10 counts s^{-1} were included in the final spectrum [SAS extraction expression (RATE > 0.5) && (RATE ≤ 10.0) && (FRACEXP > 0.7), the last expression guarantees that each bin has an exposure of at least 70 per cent].[1] Excluding data with count rates above 10 counts s^{-1} change the average flux by about 5 per cent (Fig. 1, right). These changes are highest in the lower energy band, which dominates the overall source spectrum and is therefore the spectral part which is crucial for determining the spectral parameters. The light curves were extracted in the same manner, except that we dropped the condition (RATE ≤ 10.0).

[1] This selection is not fulfilled for 2.4 (Revs 1491–1494) and 5.3 per cent (Revs 1971–1974) of these time bins.

We note that since the publication of the earlier *XMM–Newton* observation of 1H 0707−495 (Fabian et al. 2009; Zoghbi et al. 2010) the calibration of the EPIC-pn has significantly changed in the soft X-rays (3 per cent below 0.6 keV, see Fig. 1, left). The newer response is now in line with simultaneous measurements from the RGS (see XMM-CCF-REL-266, available at http://xmm2.esac.esa.int/external/xmm_sw_cal/calib/rel_notes/index.shtml). In order to take into account any remaining systematic uncertainties in the complex spectral models as well as any remaining calibration uncertainty, a systematic error of 3 per cent is added to data taken below 1.2 keV.

The RGS spectra were processed with the SAS task RGSPROC with calibration files created 2011 mid April. The observations were screened for high background times in the standard way and run with the RGS rectification on (see XMM-CCF-REL-269, available at http://xmm2.esac.esa.int/external/xmm_sw_cal/calib/rel_notes/index.shtml), which allows a direct comparison with EPIC-pn results.

Simultaneously to the *XMM–Newton* observations, between 2010 September 12 and 2010 September 19, we also observed 1H 0707−495 with the *Chandra* satellite (Canizares et al. 2005) for a total of 118.2 ks (Obs ID 12115, 12116, 12117 and 12118). The medium and high energy transmission gratings (METG and HETG) spectra were extracted and the grating auxiliary response files (ARFs) and response matrix files (RMFs) were created using the standard CIAO threads (v4.1) and CALDB (v4.1.2). The spectra for each observation and for the +1 and −1 orders were then combined using standard CIAO scripts.

Spectral fitting was performed with the Interactive Spectral Interpretation System (ISIS; Houck & Denicola 2000). Data were rebinned to oversample the intrinsic energy resolution of the EPIC-pn slightly, requiring a rebinning to 2, 3, 10, 15 and 25 bins for energies above 0.8, 2.0, 4.0 and 7.0 keV, respectively, where one bin has a width of 5 eV. Where necessary, data were rebinned further in order to reach a signal-to-noise ratio (S/N) of >2.5. All uncertainties are given at 90 per cent confidence if not stated differently.

3 THE X-RAY SPECTRUM OF 1H 0707−495

3.1 Introduction

1H 0707−495 is known from previous observations to be a highly variable Narrow-Line Seyfert 1 galaxy (Leighly 1999; Turner et al. 1999). Fig. 2 shows the light curve and hardness ratio during the observation in Revs 1491–1494 and Revs 1971–1974. In comparison the older observation (Revs 1491–1494) was a little less variable (rms variability of 6 per cent compared to 9 per cent for 100 s bins) and slightly weaker (4.6 counts s^{-1} in average compared to 5.1 counts s^{-1}). In combination with the hardness–intensity diagram (Fig. 3), where no distinct difference between the two observations can be seen, it is obvious that the source was in a similar state. Nevertheless, this diagram reveals that data from the newer observation are slightly softer (mean hardness ratio of 0.030 compared to 0.038). In Section 3.3, we will show that the softening originates from a softer power-law index and a stronger soft excess, but does not influence other fitting parameters significantly.

Fig. 4 compares the unfolded spectra of Revs 1491–1494 and Revs 1971–1974. Apart from the overall similar spectral shape, a large number of the smaller spectral features are similar, including the 'wiggles' in the 2–5 keV band that have been attributed to the complex emission and absorption spectrum of the source (Blustin

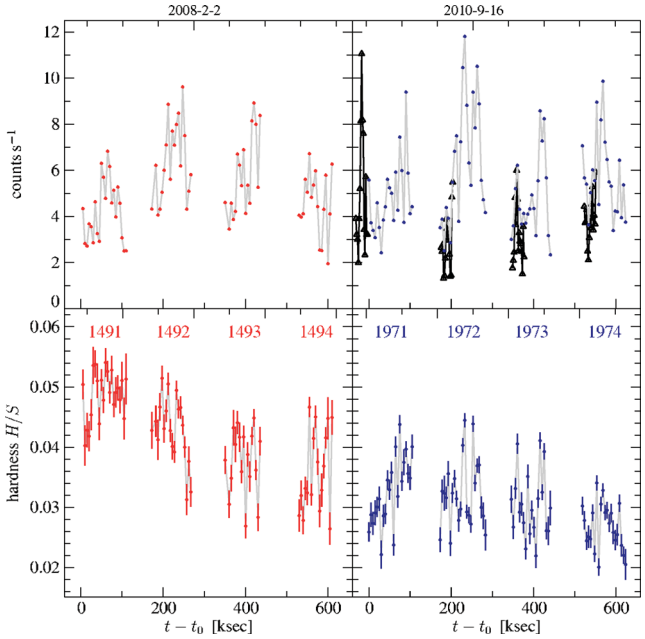

Figure 2. Left: light curve of the measurements analysed by Zoghbi et al. (2010) (Revs 1491–1494, red). Right: light curve from the 2010 September observations (Revs 1971–1974, blue). Both light curves are binned to a time resolution of 5 ks for the energy band 0.3–10.0 keV. In addition, the simultaneous *Chandra* light curve for 0.35–8.0 keV is shown below the *XMM–Newton* light curve (black, triangles). Because of lower count rate, the rate was multiplied by a factor of 50 for comparison. Bottom panels: X-ray hardness for both observations. S and H denote source counts in the bands 0.35–1.5 and 2.0–8.0 keV, respectively.

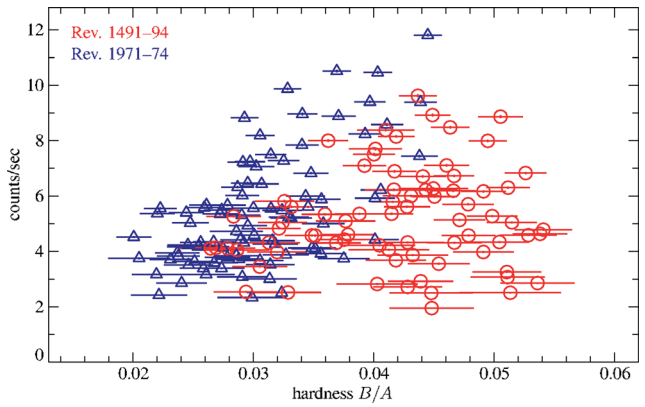

Figure 3. Hardness–intensity diagram of the observations, based on a time resolution of 5 ks. The new observation (Revs 1971–1974, blue triangles) is slightly but significantly softer than Revs 1491–1494 (red circles). There is a positive correlation between the hardness and the intensity, which is stronger for Revs 1971–1974 (correlation coefficient $\rho = 0.60$) than for Revs 1491–1494 ($\rho = 0.23$).

& Fabian 2009). Moreover, the characteristic drop at ∼7 keV is observed at the same energy. At energies above this spectral drop, more flux is missing than can be explained by a simple softening of the source. As will be shown in Section 3.5, this difference might be due to variability of an ultrafast and highly ionized wind, which acts as an absorber.

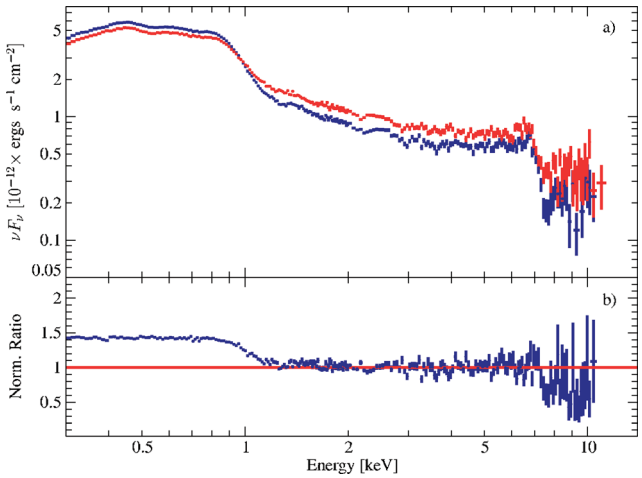

Figure 4. (a) Unfolded spectra of Revs 1491–1494 (red) and Revs 1971–1974 (dark blue). The bottom panel (b) shows the ratio of the unfolded spectra (Revs 1971–1974 divided by Revs 1491–1494). It demonstrates that the new observation becomes softer, but most spectral features remain the same. For illustrative purposes the ratio spectrum was multiplied by a constant factor such that the 2–5 keV range coincides with unity.

3.2 Broad-band spectrum and absorption

We model the average X-ray continuum using the standard spectrum for Narrow-Line Seyfert 1 spectra, namely, a steep, absorbed power-law spectrum plus (relativistically smeared) X-ray reflection (e.g. Vaughan et al. 1999; La Mura et al. 2011). Initially, foreground X-ray absorption was modelled assuming a equivalent column of $N_{\rm H} = 4 \times 10^{20}\,{\rm cm}^{-2}$ as obtained from the full resolution data of the Leiden–Argentine–Bonn 21-cm survey (LAB survey; Kalberla et al. 2005) and assuming the abundances of Wilms, Allen & McCray (2000). After adding a weak soft excess modelled by a disk blackbody (Mitsuda et al. 1984; Makishima et al. 1986) with a temperature of $kT_{\rm in} \sim 100\,{\rm eV}$, we obtain a basic model which describes the EPIC-pn data well, although below 0.5 keV, some residuals remain. One explanation for these residuals is additional source intrinsic absorption at a level of $\sim 3 \times 10^{20}\,{\rm cm}^2$. An increased column in this range is necessary to obtain any good fit at all when extending the lower end of the spectrum to 0.3 keV. If true, however, at this column a resonant O I Kα line at 0.527 keV in the rest frame of the source should be visible, i.e. at 0.506 keV in the measured spectrum, which is not the case (Fig. 5). A systematic grid search for any other narrow line associated with a potential absorber failed as well. Any increased neutral $N_{\rm H}$ must therefore be of Galactic origin. We note that like most 21 cm $N_{\rm H}$ values quoted in X-ray astronomy, the $N_{\rm H}$ value quoted above is from an all-sky 21-cm survey with a rather coarse angular resolution of 0.°6 such that small-scale variations of $N_{\rm H}$ are washed out. Within 3° of 1H 0707−495, the LAB survey contains points with $N_{\rm H}$ as large as $8 \times 10^{20}\,{\rm cm}^{-2}$. In addition, 21-cm data only probe the gas phase of the interstellar medium, while a significant amount of X-ray absorbing material could also be in molecules. It is not uncommon for higher Galactic latitudes that the gas and molecular columns are comparable ($N({\rm H}_2)/N({\rm H})$ varies between 0.2 and 5 in the sample of Magnani, Blitz & Mundy 1985). Finally, it cannot be ruled out that some of the excess absorption is source intrinsic and either in mildly ionized material or in material that is fast enough that narrow features are smeared out as suggested by Zoghbi et al. (2010). We therefore leave $N_{\rm H}$ as a free parameter in our spectral modelling and do not speculate on the relative fraction of source intrinsic and

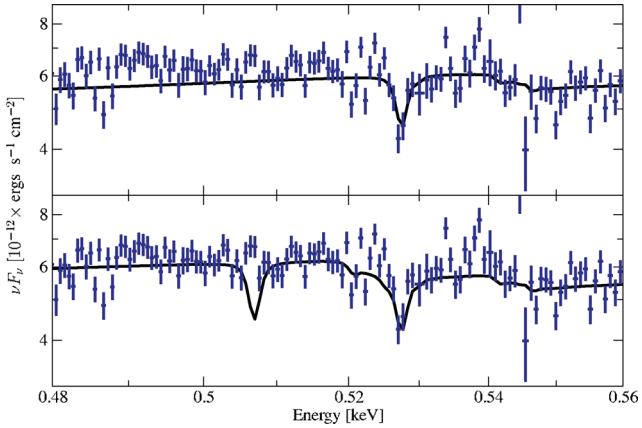

Figure 5. The EPIC-pn best fit applied to the RGS spectra of Revs 1971–1974 and focusing on the O I (0.527 keV) absorption line. The upper panel shows the best-fitting model for Galactic absorption only. The absorption line is clearly seen in the data. Residuals from a better fit including source intrinsic absorption ($z = 0.04057$) are shown in the lower panel. The lack of a redshifted O I line at 0.506 keV in the measured spectrum shows that the additional neutral absorption is not source intrinsic.

Galactic absorption along the line of sight to 1H 0707−495 from these fits.

3.3 Reflection model

For the detailed modelling of the spectrum we started with the single reflection model as proposed as best-fitting model by Fabian et al. (2009) and Zoghbi et al. (2010). This model consists of ionized reflection from an accretion disc (REFLIONX; Ross & Fabian 2005, 2007), which is relativistically smeared using the RELCONV model (Dauser et al. 2010). In addition, a weak disk blackbody with $kT_{\rm in} \sim 100$ eV was added to describe the soft excess.

In this model, relativistic smearing is parametrized using the emissivity law $\epsilon(r)$ of the accretion disc, which describes the radius-dependent reflected power of the accretion disc per unit area (Dauser et al. 2010, and references therein). Initially, $\epsilon(r)$ was described by a broken power law. Extensive spectral analysis showed, however, that the parameters for describing such an emissivity, two spectral indices and the break radius, were only poorly constrained when allowed to vary freely. As suggested for 1H 0707−495 by Wilkins & Fabian (2011) and Fabian et al. (2012) and for Narrow-Line Seyfert 1 galaxies in general by Ghisellini, Haardt & Matt (2004), we therefore constrain the emissivity to be due to the lamp-post geometry (Martocchia & Matt 1996). In this accretion geometry, the X-ray continuum is produced by a compact and central source above the black hole which focuses (part of) the radiation on to the accretion disc, which extends from the innermost stable circular orbit out to $400\,r_{\rm g}$, where $r_{\rm g} = GM/c^2$ is the gravitational radius. In this model, the only free parameter determining the emissivity profile is the height of the point-like source of X-rays above the black hole. As the emissivity in the lamp-post geometry can also be approximated by a broken power law to zeroth order (see e.g. fig. 11 of Fabian et al. 2012), we were easily able to reproduce any good fit in the lamp-post geometry with an equally good one for a broken power-law emissivity.

This model is capable of roughly describing the data (χ^2/dof = 359/220 $\sim$ 1.63 and 503/214 $\sim$ 2.35 for Revs 1491–1494 and Revs 1971–1974, respectively), with relativistic parameters for both observations being similar to Zoghbi et al. (2010). Fig. 6(b) shows

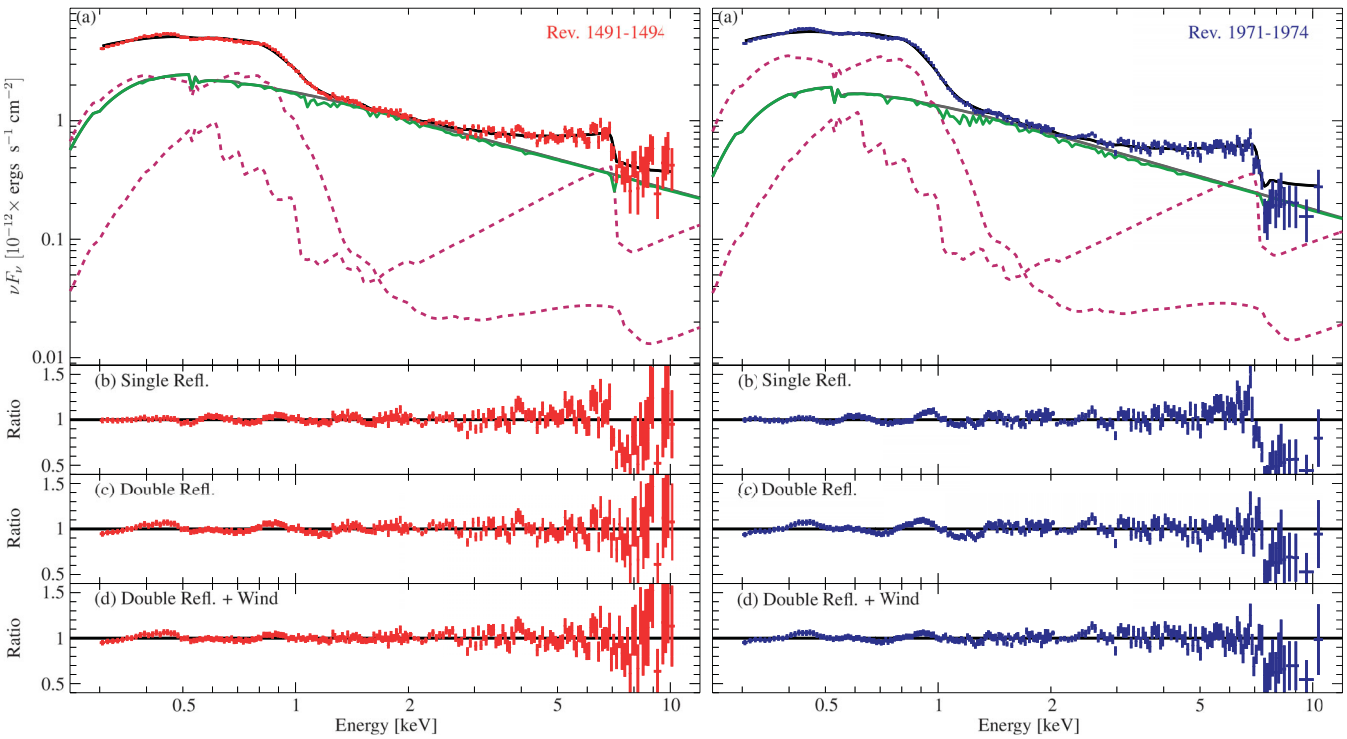

Figure 6. Best-fitting model of Revs 1491–1494 (left) and Revs 1971–1974 (right). (a) The upper panel shows the best-fitting model components: two relativistic reflection components (purple, dashed) and a power law (dark grey), absorbed by a highly ionized and blueshifted outflow (green). The lower panels show the residuals of (b) a single reflection component, (c) two reflection components and (d) the best-fitting model with additional absorption by an ionized wind.

Table 1. Best-fitting models, as shown in Fig. 6: Model 1 is a power law, a single broadened reflection component and a blackbody. Model 2 consists of two reflection components of different ionization parameter, ξ, and Model 3 is the best-fitting model, based on Model 2 combined with absorption of radiation in a highly ionized wind. The ionization parameter is defined as $\xi = 4\pi F/n_e$, with flux, F, and electron number density, n_e. The parameter v_{swind} is the velocity dispersion of the wind and z_{swind} its redshift compared to the rest frame. Note that in most models, the iron abundance relative to solar in the REFLIONX component, Z_{Fe}, pegs at the upper limit of $Z_{Fe} = 20$, while all other elemental abundances are fixed to solar.

	Model 1 (single refl.)		Model 2 (double refl.)		Model 3 (double refl. + wind)	
	Revs 1491–1494	Revs 1971–1974	Revs 1491–1494	Revs 1971–1974	Revs 1491–1494	Revs 1971–1974
$A_\Gamma \times 10^{-3}$	$0.958^{+0.017}_{-0.029}$	$0.727^{+0.013}_{-0.014}$	$1.093^{+0.023}_{-0.031}$	$0.836^{+0.018}_{-0.020}$	$1.182^{+0.030}_{-0.027}$	$0.913^{+0.024}_{-0.025}$
Γ	$2.575^{+0.032}_{-0.022}$	$2.609^{+0.025}_{-0.020}$	$2.86^{+0.04}_{-0.05}$	2.91 ± 0.04	$2.86^{+0.05}_{-0.04}$	$2.853^{+0.027}_{-0.025}$
$A_{refl_1} \times 10^{-5}$	$0.096^{+0.032}_{-0.025}$	$0.088^{+0.026}_{-0.016}$	$2.0^{+0.6}_{-0.5}$	$2.7^{+0.7}_{-0.4}$	$3.6^{+0.4}_{-1.4}$	$4.8^{+0.6}_{-2.0}$
$A_{refl_2} \times 10^{-5}$	–	–	$0.0058^{+0.0018}_{-0.0010}$	$0.0111^{+0.0013}_{-0.0010}$	$0.0056^{+0.0010}_{-0.0007}$	$0.0048^{+0.0013}_{-0.0008}$
$\log(\xi_{Refl_1})$	$1.965^{+0.059}_{-0.030}$	$2.074^{+0.027}_{-0.022}$	$1.301^{+0.014}_{-0.148}$	$1.301^{+0.010}_{-0.109}$	$1.00^{+0.14}_{-0.00}$	$1.004^{+0.251}_{-0.004}$
$\log(\xi_{Refl_2})$	–	–	$2.995^{+0.012}_{-0.115}$	$3.000^{+0.004}_{-0.051}$	$3.000^{+0.027}_{-0.081}$	$3.301^{+0.006}_{-0.118}$
Z_{Fe}	$19.73^{+0.28}_{-11.54}$	$20.0^{+0.0}_{-1.0}$	$10.3^{+3.4}_{-2.5}$	$12.0^{+2.8}_{-2.5}$	15 ± 5	20^{+0}_{-6}
h^{lp} (r_g)	29^{+8}_{-5}	$3.0^{+0.6}_{-0.0}$	$3.13^{+0.71}_{-0.13}$	$3.00^{+0.28}_{-0.00}$	$3.0006^{+0.3372}_{-0.0006}$	$3.00^{+0.13}_{-0.00}$
a^{lp}	$1.0^{+0.0}_{-1.2}$	$0.971^{+0.016}_{-0.017}$	$0.998^{+0.000}_{-0.009}$	$0.9980^{+0.0000}_{-0.0023}$	$0.998^{+0.000}_{-0.008}$	$0.998^{+0.00}_{-0.011}$
θ^{lp} (°)	$77.7^{+2.3}_{-4.8}$	$58.4^{+0.9}_{-1.3}$	$48.8^{+1.4}_{-1.9}$	48.8 ± 1.0	$52.0^{+1.7}_{-1.8}$	$48.8^{+1.3}_{-1.2}$
N_H (10^{22} cm^{-2})	$0.070^{+0.019}_{-0.009}$	0.082 ± 0.010	$0.052^{+0.004}_{-0.005}$	$0.0589^{+0.0024}_{-0.0025}$	$0.0545^{+0.0027}_{-0.0030}$	$0.0628^{+0.0025}_{-0.0028}$
$A_{bb} \times 10^4$	$0.59^{+1.07}_{-0.19}$	$1.7^{+1.0}_{-0.7}$	–	–	–	–
kT_{bb} (eV)	112^{+8}_{-17}	96^{+7}_{-6}	–	–	–	–
N_H^{swind} (10^{22} cm^{-2})	–	–	–	–	$3.6^{+7.0}_{-0.6}$	$4.0^{+1.3}_{-1.0}$
$\log(\xi_{swind})$	–	–	–	–	$3.61^{+0.17}_{-0.07}$	$3.299^{+0.024}_{-0.071}$
v_{swind} (c)	–	–	–	–	≤ 0.025	≤ 0.014
z_{swind}	–	–	–	–	$-0.063^{+0.015}_{-0.007}$	$-0.1262^{+0.0015}_{-0.0036}$
χ^2/dof	$359/220 = 1.63$	$503/214 = 2.35$	$290/220 = 1.32$	$439/214 = 2.05$	$237/216 = 1.10$	$274/210 = 1.31$

the corresponding fit and residuals, Table 1 lists the best-fitting parameters. We note that the best-fitting values of height and inclination for Revs 1491–1494 differ significantly from those values obtained in the other models. However, there exists some degeneracy between the best-fitting values for these parameters, as the model only roughly describes the data. Therefore the fit is found to be almost as good, when the height and inclination are fixed to the best-fitting values obtained for the other fits.

Especially for Revs 1971–1974, the sharp drop in the spectrum at ∼7 keV is not well modelled by a single reflection. Using a second reflection component, which is highly ionized, significantly improves the fit ($\Delta\chi^2$(Revs 1971–1974) = 64, Fig. 6c). This second reflection component acts as an additional layer on top of the moderately ionized component, i.e. the reflectors are not radially separated. In this composite model, emission from the highly ionized reflection component at low energies describes the soft excess, i.e. an additional blackbody component is not required, while the low ionized reflection with strong Kα emission line accounts properly for the strong drop in flux around 7 keV.

Even in this two component reflection fit, however, some residuals remain in the area around ∼1 keV, especially for Revs 1971–1974. These residuals can be described by a highly ionized ($\log(\xi) \sim 3.5$) and smeared outflow, modelled here using the SWIND model (Gierliński & Done 2004, see Fig. 6d and green line in Fig. 6a). Particularly for Revs 1971–1974, such an absorption improves the fit a lot ($\Delta\chi^2 = 165$). Moreover, the blueshifted absorption of Fe XXV and Fe XXVI at 6.7 and 7.0 keV is automatically predicted at the position of the prominent absorption feature at ∼7.5 keV seen directly below the sharp drop. The SWIND model describes the remaining residuals in a satisfactory manner, with outflow velocities of $0.18 \pm 0.01\,c$ and $0.11 \pm^{+0.01}_{-0.02}\,c$ for Revs 1971–1974 and Revs 1491–1494, respectively, calculated from the determined redshift parameter z_{swind} (see Table 1). Winds at these speeds are commonly seen in many sources (see e.g. Tombesi et al. 2010). We will discuss this result in greater detail below (Section 3.5). In addition, the smearing due to a turbulent velocity is in the order of 0.01 c–0.02 c, i.e. 3000–6000 km s^{-1}, which is in agreement with the gratings spectrum (see Section 3.2). Despite this overall success of the model, however, the predicted strength of these lines is too weak. This weakness is a limitation of the SWIND model, which is constrained to material of solar abundances and does not allow us to model these lines using the extreme metallicity indicated by the reflection component.

Despite the large uncertainties, at each point above 7 keV in Revs 1971–1974 there is a systematic overprediction of the flux (see Fig. 6d, right). It probably originates from improperly modelled accretion disc reflection; in particular, contributions from the lower ionized component contribute to a large amount of the total flux observed in this energy range (see Fig. 6a). As will be discussed in detail in Section 4, the modelling of the reflection suffers from several constraints. For example, the simplified modelling of the accretion disc spectrum, or the fact that Fe is highly overabundant while all other elements are at solar abundance, could easily produce an overprediction of the model flux above 7 keV. In addition to that, the mildly ionized wind we find can only be modelled assuming solar composition, too, although we conclude from the reflection component that Fe is highly overabundant. We therefore expect that our model underpredicts the absorption by H- and He-like transitions of iron in the energy range around 7 keV.

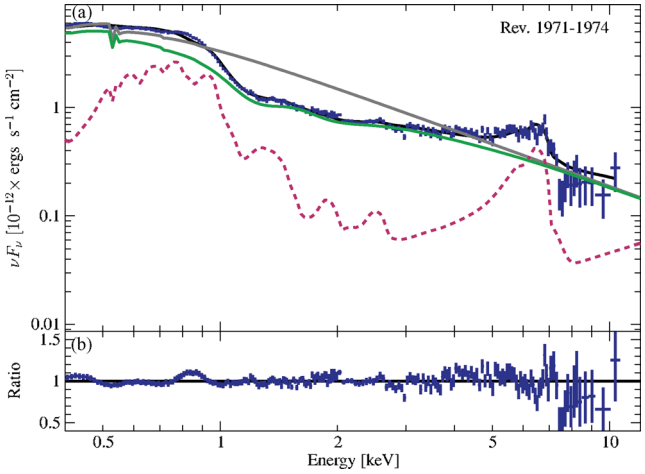

Figure 7. An alternative model (here for Revs 1971–1974) which describes the soft excess as a blend of several mildly ionized ($\log(\xi) \sim 2.2$) and smeared oxygen absorption lines. (a) Single components: the effect of the absorption on the original power law (dark grey) is illustrated by the green line and the reflection component is shown by the purple, dashed line. (b) Residuals of the best fit (χ^2/dof = 375/226 ∼ 1.66).

3.4 Alternative models: smeared absorption

As an alternative to the 'pure' reflection model, we also tried to model the soft excess by a strongly ionized and ultrafast outflow in a manner proposed by Gierliński & Done (2004). As discussed in Section 3.2, there are no narrow lines present in the RGS spectrum of 1H 0707−495. We therefore use again the SWIND model to describe smeared absorption. Fig. 7 shows that this model together with a single reflection component is capable of describing the data. Compared to the residuals in Fig. 6, however, the emission-like hump around 0.9 keV is much more pronounced. In order to work, the model requires an outflow velocity of ∼0.37 c of the absorbing material, which is larger than most relativistic outflows observed in active galaxies (see e.g. Blustin et al. 2005; Tombesi et al. 2010). More doubtful is that in order to explain the data a line broadening with a rms velocity distribution of as high as 50 000 km s^{-1} has to be assumed. From a statistical point of view, however, this model cannot be completely rejected (χ^2/dof = 375/226 ∼ 1.66 for Revs 1971–1974).

Finally, as argued by Zoghbi et al. (2010), if the spectral drop was due to a partially covering absorber a strong neutral K line would be expected. For the upper limit search we use the summed *Chandra* HETG spectrum without any further binning. With these observations we are able to determine the upper limit of the flux of a narrow ($\sigma = 1$ eV) Gaussian line at 6.4 keV to $F_{6.4} < 2.0 \times 10^{-6}$ photons s^{-1} cm^{-2} at 90 per cent confidence. This upper limit is consistent with our EPIC-pn spectral modelling, but does not allow to constrain the modelling further. The absence of this line again argues against the absorption interpretation.

3.5 A highly ionized outflow in 1H 0707−495

A highly ionized and fast outflow was already used by Done et al. (2007) to describe the spectrum of 1H 0707−495, where strong absorption in this wind models the complete spectral shape, including the sharp drop at ∼7 keV as a P Cygni line. In contrast, in our best-fitting model the main spectral features (the soft excess and the sharp drop) are described by reflection, while the wind, being more ionized, has a smaller influence on the observed spectrum. We

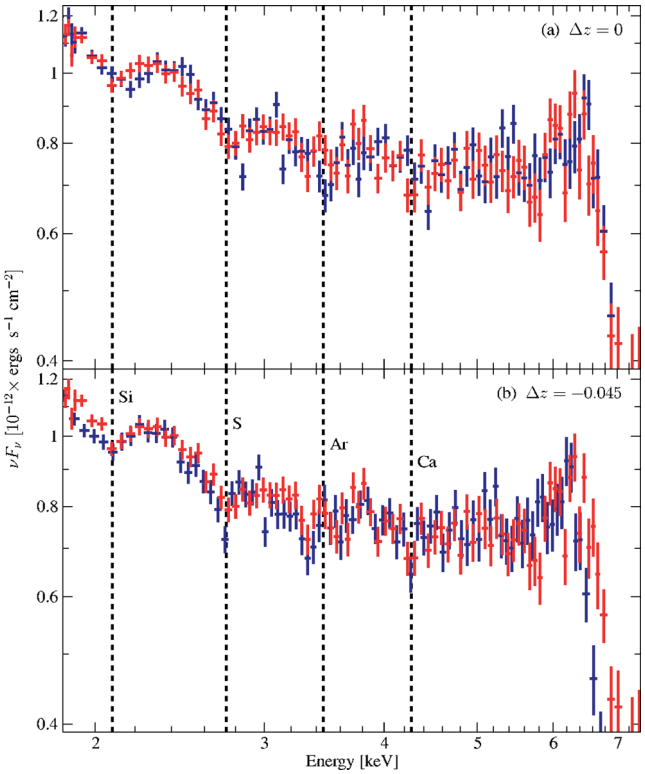

Figure 8. (a) A zoom into the hard X-ray bandpass of the spectra: for illustrative purposes Revs 1971–1974 (dark blue) is renormalized to the same νF_ν in the 2–5 keV band as Revs 1491–1494 (red). Energies are given in the rest frame of the source. (b) Here we apply a manual energy shift to Revs 1971–1974 (blue) corresponding to a redshift of $\Delta z = z_{\mathrm{Revs\,19}} - z_{\mathrm{Revs\,14}} = -0.045$, which leads to the best agreement for most absorption-like features that are seen consistently in both observations. The most prominent of these features are indicated by dashed lines. Assuming an outflow velocity in Revs 1491–1494 of ∼0.04 c they can be attributed to 1s–2p transitions of H-like Si, S, Ar and Ca.

saw in Section 3.3 that a major difference between Revs 1491–1494 and Revs 1971–1974 is a difference of ∼0.07 c in wind velocity. Comparing the two spectra for the higher energetic range (Fig. 8a) reveals that of all the structure seen in this energy band only the steep drop around ∼7 keV agrees in both observations. This constancy is expected if the 7 keV feature is due to a relativistic line emitted from an accretion disc. If one wanted to explain the full spectrum by absorption, however, it would be very unlikely that all spectral features except for the drop change their location and that only the strongest feature stayed constant.

Taking a closer look at the spectra away from the 7 keV feature reveals that indeed the same features appear in both observations, but they are slightly shifted in energy. Correcting for this shift 'by eye' we find that most features agree nicely if the shift is approximately $\Delta z = z_{\mathrm{Revs\,19}} - z_{\mathrm{Revs\,14}} \sim -0.045$ (Fig. 8b). This relative shift is consistent with the difference in redshift found between the two swind components obtained by spectral modelling, $\Delta z_{\mathrm{swind}} = -0.06^{+0.01}_{-0.02}$. We therefore attribute the fine spectral structure between 2 and 5 keV to a fast and highly ionized outflow.

Assuming redshifts of $z_{\mathrm{Revs\,14}} = -0.04$ and $z_{\mathrm{Revs\,19}} = z_{\mathrm{Revs\,14}} + \Delta z = -0.085$, the structures in the spectrum can tentatively be identified with single 1s–2p transitions of H-like Si, S and Ca (Fig. 8b). Again, the individual redshifts found by eye agree with the ones found in our spectral fits for the two swind components, $-0.06^{+0.02}_{-0.01}$

and -0.13 ± 0.01. In such a highly ionized plasma we would also expect a strong resonant transition from argon. Inspection of the Ar band reveals a feature that is more complex than the absorption features in the Si, S and Ca band, making its interpretation difficult at the resolution of an X-ray CCD. A possible explanation could be a P Cyg profile of H-like Ar, however, in this case Ar would have a different redshift than the other features, which seems unlikely. We note, however, that the overall shape of this feature remained stable between both observations. Further modelling of the spectral features using proper wind models is therefore required, which is outside of the scope of this paper.

4 SUMMARY AND DISCUSSION

In this paper we have presented the results from a spectral analysis of 500 ks of new *XMM–Newton* and *Chandra* data from the AGN 1H 0707−495 and have compared these results to the previous long observation of the source. In agreement with earlier work (Fabian et al. 2009, 2012; Zoghbi et al. 2010), the simple picture deduced from these observations is that 1H 0707−495 an accretion disc around a maximally rotating black hole is irradiated by a central and compact source closely above the black hole, producing the underlying complex X-ray continuum by reflection. In both observations, the primary X-ray source which irradiates the accretion disc has a height of $\leq 4\, r_{\rm g}$ above the black hole. Such a low emitter is in line with timing measurements (Zoghbi et al. 2010) and implies that the photons are extremely focused on to the inner parts of the disc. Fits with an empirical broken power-law emissivity confirm this interpretation ($\epsilon_{r<r_{\rm br}} = 10.2^{+0.8}_{-0.9}$, $\epsilon_{r>r_{\rm br}} = 2.3^{+0.5}_{-0.1}$, $r_{\rm br} = 2.9^{+0.2}_{-1.0}\, r_{\rm g}$ for Revs 1971–1974). Despite significant changes in the continuum shape between both observations, the black hole in 1H 0707−495 is consistently well determined to be maximally rotating. This result also adds further credibility to the relativistic line interpretation of the spectrum, as the black hole parameters are not expected to change on such short time-scales. Such a behaviour would be significantly more difficult to explain in alternative models explaining the line via an ionized and blueshifted radial wind.

The accretion disc causing the observed reflection features has a complex ionization structure, which is here approximated by two reflectors of strongly different ionization as modelled by Ross & Fabian (2005, 2007). Even though the highly ionized reflector dominates the soft X-ray spectrum, its normalization is only 0.1–0.2 per cent of that of the weakly ionized reflector, i.e. most of the irradiated X-rays are intercepted by the colder medium. This result fits nicely into the picture of a rather neutral accretion disc with a thin skin of highly ionized material caused by the incident X-rays (see e.g. García & Kallman 2010; García, Kallman & Mushotzky 2011). As a caveat, however, note that our approach implicitly assumes that the ionization fraction of the disc is independent of distance from the black hole. From basic arguments it is clear that the photoionization due to the incident X-rays will result in an ionization structure of the disc surface which strongly depends on radius, as even in the simplest and most conservative models photons are strongly focused towards the inner parts. Additionally, the energy release within the accretion disc itself will give rise to a temperature and ionization gradient (e.g. Hubeny et al. 2001; Davis et al. 2005, and references therein).

As shown by our modelling of the weaker spectral features, the relativistically blurred continuum is then modified by absorption in an ultrafast wind (0.11–0.18 c, i.e. 30 000–50 000 km s^{-1}). Because of the change of the minor features at 2–5 keV and the constancy of the 7 keV drop between the two observations (see Section 3.5), the ionized wind could be uniquely identified to exist along with the reflection, which dominates the spectrum. The overall properties of this wind are in line with the relativistic, highly ionized winds that have now been detected in more than 40 radio-quiet AGN, including Narrow-Line Seyfert 1 galaxies. These winds have been mainly detected through strongly redshifted Kα and Kβ absorption lines from H- and He-like iron. See e.g. Chartas et al. (2002), Pounds et al. (2003), Turner, Kraemer & Reeves (2004) or Cappi et al. (2009) for discussions of individual sources and Tombesi et al. (2010) for a recent comprehensive study with *XMM–Newton*.

Radiation hydrodynamical calculations show that such winds can in principle be formed as line-driven winds from an accretion disc (Proga, Stone & Kallman 2000; Kurosawa & Proga 2009, and references therein). The spectral signature imprinted on an X-ray continuum is in rough agreement with the features seen here (e.g. Schurch, Done & Proga 2009), although further theoretical work such as proper inclusion of Compton broadening is clearly needed (e.g. Sim et al. 2010). Unfortunately, the current wind models available for X-ray spectral modelling also do not yet allow us to self-consistently model absorption with abundances consistent with the significant overabundance in the accreted material inferred from the X-ray reflection. Despite this problem, however, the agreement between our simple wind model and the data is remarkable. In passing, we note that the measured outflow velocity is also consistent with the unified model for quasars proposed by Elvis (2000), where a 'warm highly ionized medium' is ejected at speeds of 10 000–60 000 km s^{-1} at an inclination of around 60°. Coincidentally, this value is in agreement with our best-fitting inclination angle. Note that in order to explain the apparent shift of minor spectral features in the 2–5 keV band, the line-of-sight velocity of this wind must have changed between both observations. As such a wind is expected to be highly structured (Sim et al. 2010), only very slight changes in the line of sight would be required to explain the observed change in velocity.

Despite the overall success of the modelling, however, some significant broad residuals remain (Fig. 6d). There are several major issues which could explain these discrepancies that could not be treated properly in our analysis due to limitations of our best-fitting model (Section 3.3). First of all, while measurements of the reflection show a high Fe abundance in reflection, all other elements are assumed to be of solar abundance. From basic arguments it is clear that a high Fe abundance likely implies that other elements are overabundant as well, which could not be taken into account in our approach due to the limitations of the REFLIONX model. Such a restriction might therefore underpredict emission from other elements, while at the same time overpredict the Fe abundance. Improving on modelling the ionization gradient in the accretion disc as discussed above could also slightly reduce the artificially high Fe abundance obtained from fitting the data with simple reflection models (Reynolds, Fabian & Inoue 1995). As already discussed by Zoghbi et al. (2010), however, Narrow-Line Seyfert 1 galaxies such as 1H 0707−495 exhibit enhanced star formation (Sani et al. 2010) and therefore are expected to be Fe enriched. This assumption is confirmed in near-IR measurements (see e.g. Shemmer & Netzer 2002). Moreover, in similar sources like MCG-6-30-15 (Miniutti et al. 2007), 1H 0419−577 (Fabian et al. 2005) or IRAS 13224−3809 (Ponti et al. 2010) iron is also required to be overabundant.

Regarding the ionized wind seen in absorption, we measure a lower wind velocity and $N_{\rm H}$ compared to earlier absorption-dominated models (Gallo et al. 2004; Done et al. 2007). This difference is probably due to the fact that in earlier models the full

continuum was seen to be dominated by the wind, while in the present model the soft excess is mainly described by reflection of a highly ionized accretion disc. This interpretation is in line with our identification of weaker spectral features as absorption lines from H-like ions (Si, S, Ca and possibly Ar), which are found at the correct energies expected from the inferred wind velocities. As discussed above, since the 7 keV feature is non-variable, it cannot be due to the wind. This result significantly simplifies the wind modelling, as in order to explain the whole 7 keV feature as a wind a very complex absorber is necessary (see also Done et al. 2007, note, however, that the ionized and blueshifted absorption is required to describe the narrow absorption feature right above the drop).

ACKNOWLEDGMENTS

This work is based on observations obtained with *XMM–Newton*, an ESA science mission with instruments and contributions directly funded by ESA Member States and NASA. JW and TD acknowledge partial support from the European Commission under contract ITN 215212 'Black Hole Universe' and TD by a fellowship from the Elitenetzwerk Bayern. JS acknowledges support from the Grant Agency of Czech Republic (GACR 202/09/0772). We thank John Davis for the development of the SLXFIG module used to prepare the figures in this paper, and Alex Markowitz and Moritz Böck for their many useful discussions.

REFERENCES

Blustin A. J., Fabian A. C., 2009, MNRAS, 399, L169
Blustin A. J., Page M. J., Fuerst S. V., Branduardi-Raymont G., Ashton C. E., 2005, A&A, 431, 111
Boller T. et al., 2002, MNRAS, 329, L1
Boller T., Tanaka Y., Fabian A., Brandt W. N., Gallo L., Anabuki N., Haba Y., Vaughan S., 2003, MNRAS, 343, L89
Canizares C. R. et al., 2005, PASP, 117, 1144
Cappi M. et al., 2009, A&A, 504, 401
Chartas G., Brandt W. N., Gallagher S. C., Garmire G. P., 2002, ApJ, 579, 169
Dauser T., Wilms J., Reynolds C. S., Brenneman L. W., 2010, MNRAS, 409, 1534
Davis S. W., Blaes O. M., Hubeny I., Turner N. J., 2005, ApJ, 621, 372
den Herder J. W. et al., 2001, A&A, 365, L7
Done C., Sobolewska M. A., Gierliński M., Schurch N. J., 2007, MNRAS, 374, L15
Elvis M., 2000, ApJ, 545, 63
Fabian A. C., Miniutti G., Iwasawa K., Ross R. R., 2005, MNRAS, 361, 795
Fabian A. C. et al., 2009, Nat, 459, 540
Fabian A. C. et al., 2012, MNRAS, 419, 116
Gallo L. C., Tanaka Y., Boller T., Fabian A. C., Vaughan S., Brandt W. N., 2004, MNRAS, 353, 1064
García J., Kallman T. R., 2010, ApJ, 718, 695
García J., Kallman T. R., Mushotzky R. F., 2011, ApJ, 731, 131
Ghisellini G., Haardt F., Matt G., 2004, A&A, 413, 535
Gierliński M., Done C., 2004, MNRAS, 349, L7
Houck J. C., Denicola L. A., 2000, in Manset N., Veillet C., Crabtree D., eds, ASP Conf. Ser. Vol. 216, Astronomical Data Analysis Software and Systems IX. Astron. Soc. Pac., San Francisco, p. 591
Hubeny I., Blaes O., Krolik J. H., Agol E., 2001, ApJ, 559, 680
Jansen F. et al., 2001, A&A, 365, L1
Jones D. H. et al., 2009, MNRAS, 399, 683
Kalberla P. M. W., Burton W. B., Hartmann D., Arnal E. M., Bajaja E., Morras R., Pöppel W. G. L., 2005, A&A, 440, 775
Kurosawa R., Proga D., 2009, MNRAS, 397, 1791
La Mura G., Ciroi S., Cracco V., Ilic D., Popovic L., Rafanelli P., 2011, in Foschini L., Colpi M., Gallo L., Grupe D., Komossa S., Leighly K., Mathur S., eds, Proc. Sci. Vol. NLS1, Narrow-Line Seyfert 1 Galaxies and Their Place in the Universe. p. 56
Leighly K. M., 1999, ApJS, 125, 297
Magnani L., Blitz L., Mundy L., 1985, ApJ, 295, 402
Makishima K., Maejima Y., Mitsuda K., Bradt H. V., Remillard R. A., Tuohy I. R., Hoshi R., Nakagawa M., 1986, ApJ, 308, 635
Martocchia A., Matt G., 1996, MNRAS, 282, L53
Miniutti G. et al., 2007, PASJ, 59, 315
Mitsuda K. et al., 1984, PASJ, 36, 741
Piconcelli E., Jimenez-Bailón E., Guainazzi M., Schartel N., Rodríguez-Pascual P. M., Santos-Lleó M., 2005, A&A, 432, 15
Ponti G. et al., 2010, MNRAS, 406, 2591
Pounds K. A., King A. R., Page K. L., O'Brien P. T., 2003, MNRAS, 346, 1025
Proga D., Stone J. M., Kallman T. R., 2000, ApJ, 543, 686
Reynolds C. S., Fabian A. C., Inoue H., 1995, MNRAS, 276, 1311
Ross R. R., Fabian A. C., 2005, MNRAS, 358, 211
Ross R. R., Fabian A. C., 2007, MNRAS, 381, 1697
Sani E., Lutz D., Risaliti G., Netzer H., Gallo L. C., Trakhtenbrot B., Sturm E., Boller T., 2010, MNRAS, 403, 1246
Schartel N., Rodríguez-Pascual P. M., Santos-Lleó M., Ballo L., Clavel J., Guainazzi M., Jiménez-Bailón E., Piconcelli E., 2007, A&A, 474, 431
Schurch N. J., Done C., Proga D., 2009, ApJ, 694, 1
Shemmer O., Netzer H., 2002, ApJ, 567, L19
Sim S. A., Proga D., Miller L., Long K. S., Turner T. J., 2010, MNRAS, 408, 1396
Strüder L. et al., 2001, A&A, 365, L18
Tanaka Y., Boller T., Gallo L., Keil R., Ueda Y., 2004, PASJ, 56, L9
Tombesi F., Cappi M., Reeves J. N., Palumbo G. G. C., Yaqoob T., Braito V., Dadina M., 2010, A&A, 521, A57
Turner T. J., George I. M., Nandra K., Turcan D., 1999, ApJ, 524, 667
Turner T. J., Kraemer S. B., Reeves J. N., 2004, ApJ, 603, 62
Vaughan S., Reeves J., Warwick R., Edelson R., 1999, MNRAS, 309, 113
Wilkins D. R., Fabian A. C., 2011, MNRAS, 414, 1269
Wilms J., Allen A., McCray R., 2000, ApJ, 542, 914
Zoghbi A., Fabian A. C., Uttley P., Miniutti G., Gallo L. C., Reynolds C. S., Miller J. M., Ponti G., 2010, MNRAS, 401, 2419

This paper has been typeset from a TEX/LATEX file prepared by the author.